Free Surface Waves in Wall-Bounded Granular Flows

Stephen L. Conway, David J. Goldfarb,† Troy Shinbrot, and Benjamin J. Glasser*

Department of Chemical & Biochemical Engineering, Rutgers University, Piscataway, New Jersey 08854

(Received 11 July 2002; published 20 February 2003)

We report free-surface waves in granular flows near boundaries in an inclined chute. The chevron-shaped traveling waves spontaneously develop at inclinations close to the angle of repose for both steady and accelerating flows. Two distinct regimes are characterized by internal angle and frequency variations. Experimental measurements indicate that subsurface circulation driven by velocity gradients near frictional walls plays a central role in the pattern formation mechanism, suggesting that wave generation is controlled by the granular analog of a fluid boundary layer.

DOI: 10.1103/PhysRevLett.90.074301 PACS numbers: 45.70.Qj, 47.54.+r, 89.75.Kd

Improved insight into mechanisms of granular flow has clear significance for solids transport and mixing processes, and for describing catastrophic geophysical events. Here, we describe surface waves that occur when a granular stream impinges on an inclined plane with vertical sidewalls. As with past work in similar geometries [1,2], examination of such phenomena can yield details of shear transmission and stress development and is relevant to conveyance in industrial chutes and other surface flows, such as inside tumbling blenders. Numerous free-stream instabilities have been revealed in chutes [3–7] and in unbounded avalanches on inclined planes [8–10]. The understanding gained echoes that from earlier studies of analogous fluid systems, such as boundary layer instabilities in flow past flat plates [11]. We extend the analogy by investigation of secondary granular flows developing near boundaries.

In Fig. 1, we show six top views near the inlet to a chute, illuminated from the side. Unsieved art sand (Clifford W. Estes Co., Inc., New Jersey) is discharged from a hopper through a circular opening and impinges on the inclined surface ≈ 30 cm upstream from the tops of these snapshots. Figures 1(a)–1(f) show the effects of decreasing chute inclination, θ. At $\theta = 35°$, the surface of the flowing sand appears smooth, except for a central longitudinal trough. At lower θ, Λ-shaped waves that we term *chevrons* spontaneously develop and rapidly translate down slope. At first, the waves are visible for only the first 20 or 30 cm of flow in the chute, becoming too faint to be observed further downstream. For $\theta \leq 32°$, the chevrons remain for the entire chute length (107 cm). At lower θ still, chevrons persist until flow stalls at $\theta \approx 24°$. Chevron appearance is insensitive to ambient conditions (20% to 70% relative humidity, ~74 °F).

The ridges of the chevrons are directed *against* the flow, and the waves are oriented to the centerline with angles, ϕ, ranging from 10° to 35°. Two distinct chevron structures appear: We designate those with streamwise wavelengths <4 cm as type *A* [Fig. 1(b)], and those with longer wavelengths as type *B* [Figs. 1(c)–1(f)]. Type *A* chevrons have lower amplitude, possess more obtuse angles, ϕ, and occur at higher chute inclination than type *B*. Moreover, type *B* chevrons vanish for θ exceeding the angle of repose, $\theta_{\text{stop}} = 31° \pm 2°$. Chevrons were characterized by interrogating digital video images to quantify wave frequency (i.e., the number of waves entering the fixed image area, averaged over 270 frames), angle ϕ, and velocity versus θ. Frequencies are plotted in Fig. 2(a), which shows type *A* are consistently more frequent than type *B*. Noting the "stick-skip"description of surface avalanches [10], Fig. 2(a) indicates that both type *A* and *B* chevrons are observed for $\theta < \theta_{\text{stop}}$, for which avalanches are not expected. At higher, metastable slopes, avalanching is possible, but type *B* chevrons are absent. Figure 2(b) shows a plot of internal angle, ϕ, vs θ, where angles for type *A* are $\phi > 20°$, and approximately double those of type *B*. Only type *B* chevrons change appreciably in shape, becoming more acute at low θ. The graphs thus reveal unambiguous differences in frequency and obliqueness between the two patterns, although each possess

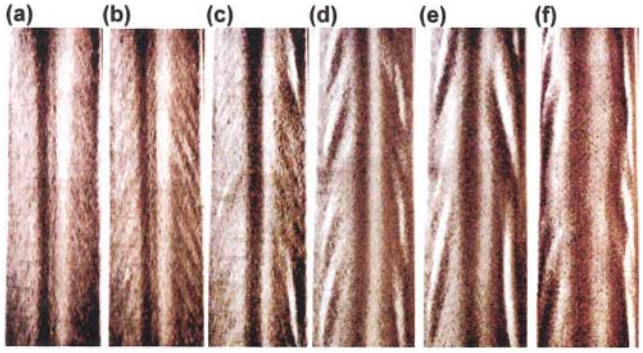

FIG. 1 (color). Chevron waves viewed from above. Flow is from top to bottom. Snapshots capture the entire width of the acrylic chute (7.6 cm), which is 107 cm long, with grounded aluminum flashing fitted into the bottom to minimize static. The steel hopper is elevated 8 cm above the chute, and also grounded. $\theta =$ (a) 33.6°, (b) 31.8°, (c) 28.7°, (d) 24.7°, (e) 24.2°, and (f) 23.5°, measured with a digital level ($\pm 0.1°$). Material mass flow $= 281 \pm 2$ g/s, tapped density 1.35 kg/m^3.

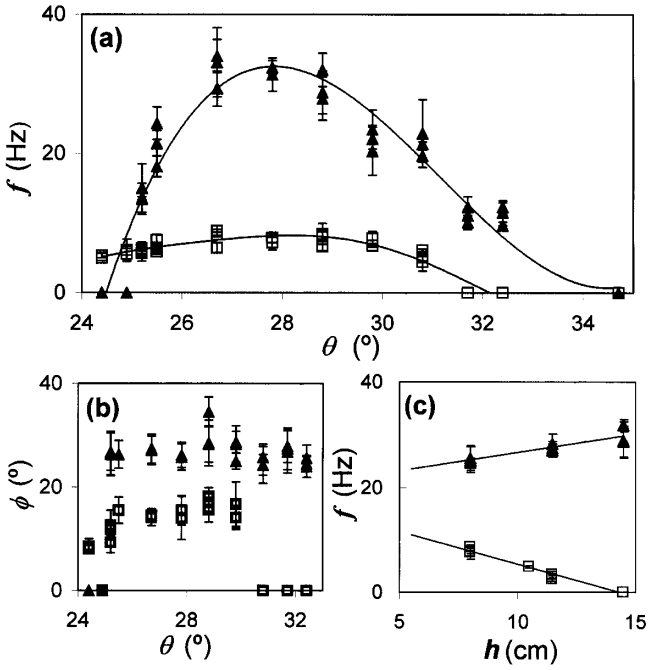

FIG. 2. Type A (triangle) and B (square) chevron characteristics. (a) Frequency vs θ. Polynomial curve fit has been added as a visual aid. $h = 8$ cm. (b) Tilt ϕ vs chute inclination, from digital stills. (c) Frequency vs h for a chute inclination 28.8°. In all cases, mass flow $= 281 \pm 2$ g/s. Error bars represent the standard deviation for each point.

comparable speed, decreasing almost linearly from 1.2 m/s (at $\theta = 33°$) to 0.8 m/s (prior to stalling).

Similar waves occur as chute width is increased from 7.6 to 20.4 cm, shown in Figs. 3(a) and 3(b). Qualitatively, this is accompanied by a transition from a fast, shallow flow (~ 3 mm bed depth) to a slower, thicker flow (7.5 to 10 mm depth). Chevrons are still apparent, albeit for a much narrower range of inclinations close to 25°, and with the left and right edges confined near the walls by a considerably broader and convex central, steady region. Near the chute entrance, where grains first impinge upon the inclined chute, the waves appear only as flow first approaches the walls. For the narrow chute width of 7.6 cm, the impingement area [Fig. 3(c)] consists of an inner, fast moving granular jet, surrounded by an outer region where grains flow more slowly [12,13]. In contrast, a transient upward propagating granular jump overcomes the inner region in the first few seconds in the wide chute. We therefore observe the wave phenomenon for two sets of entrance conditions, flow speeds, and bed depths, but only near boundaries.

The chevrons differ from previously reported granular surface patterns in several ways. Roll waves, or granular jumps [1–3,5,10,14], are characterized by curved wave fronts spanning the entire flow, oriented so that leading edges (where flow is fastest) occur near the chute centerline. By contrast, chevron vertices point uphill, are

FIG. 3 (color). Varying chute width (a) 7.6 cm and (b) 20.4 cm. (c) Grain impingement zone for 7.6 cm chute. In all cases, $\theta = 25°$, $h = 6$ cm, and mass flow $= 281 \pm 2$ g/s.

discontinuous at the centerline, and have leading edges nearest the walls. Contrasting with earlier works [1,5,14], we are unable to reproduce the chevron waves using spherical glass beads of various diameters. Here, wave frequencies range from 5 to 35 Hz, while Ref. [5] indicates wave frequencies of 0.014 to 0.3 Hz. Next, unlike previously reported longitudinal vortices [6], we only detect chevrons in *slow* flows developed at *low* inclines and on a relatively *smooth* surface. Additionally, longitudinal vortices appear 0.4 to 1.3 m downstream of the chute entrance, while the chevrons appear as flow encounters walls. Another potentially related phenomenon, V-shaped finger instabilities, are seen at avalanche fronts [4,15] and have been attributed to size segregation. Here, wave location (only near boundaries) and the degree of segregation differ. Both narrow (355–425 μm) and wide (unsieved) particle size distributions generate chevrons, and no segregation is apparent when larger, colored sand particles are introduced as tracers. Finally, patterns resembling the chevrons also occur in fluids, e.g., for cylinder wakes [16], and Λ-shaped (hairpin) vortices in boundary layers [11]. In both cases, orientation to the prevailing flow is reversed with respect to our data.

To investigate the causes of the chevron waves, we made several experimental modifications. At material flow rates below 142 ± 3 g/s (set by constricting the hopper orifice), surface waves fail to appear. Chute entrance effects were probed by altering both the shape (from circular to rectangular) and orientation of the hopper opening. This would significantly modify any waves stemming from the granular jet (cf. [17,18] for fluids), however, no change in the chevron waves was apparent. Hopper height, h, was also varied to explore initial grain energy effects [1,2]. In Fig. 2(c), we see that, as impact energy increases, type A chevrons become more frequent at the expense of type B. The opposite occurs as entrance flow is slowed: Type A are absent in the dense flows of the 20.4 cm chute. Wall properties were also modified by replacing the acrylic side walls with aluminum, which produces greater amplitude for type B chevrons, but leaves type A unchanged. Conversely, covering

the walls with coarse sandpaper widens the angle ϕ of type B chevrons, making them resemble type A (while type A is unaffected). It thus appears that a minimum flow depth is needed to sustain the chevrons, and that energetic entrance conditions and rough boundaries favor type A over type B.

Tracer particle experiments and particle image velocimetry (PIV) were performed to quantify the flow. For the narrow chute (7.6 cm), surface velocity profiles were observed using a video camera to track a transverse line formed by an aliquot of tracer particles abruptly dropped onto the flow. As previously reported [1], the line distorts and accelerates, and midstream velocities are found to exceed those nearest the walls by $\approx 50\%$. Colored sand was also used to form surface streaklines [Fig. 4(a)]. By measuring the deflection of the streaklines over the length of the chute, a small, repeatable outward lateral flow of 0.25% to 0.97% of longitudinal velocities was detected ($\pm$ 0.13%). Lateral flow was also confirmed for the 20.4 cm-wide chute; in a close-up, angled view of this chute, through transparent side walls [Fig. 4(b)], surface particles were seen to migrate toward the chute walls before submerging into the bed. Digital camera images (500 fps) yielded PIV velocity fields for exposed surface flows. Although instantaneous velocities could not be obtained for rapidly translating chevron waves in the narrow chute, averaging over 500 frames generated consistent mean velocity data [Fig. 4(c)]. These indicate a streamwise acceleration (0.15 m/s^2), and large velocity gradients near the walls (20 s^{-1}). Mean velocity is also shown in Fig. 4(d) for the near-wall region of the 20.4 cm-wide chute, showing that here steady flow is achieved—longitudinal gradients seen in the narrow chute are now absent. In addition, the deeper flows allow a velocity gradient to be measured through the transparent side walls, which is fastest near the surface, with particles decelerating upon migration towards the chute base. At the free surface, streamwise velocities are lower and so up to 50 instantaneous PIV fields can be averaged with little distortion of captured wave images; a typical pseudoinstantaneous example is shown in Fig. 4(e) where regions of vorticity are evident. Using the approach of Ref. [6], we gain insight into the out-of-plane flow by comparing streamwise (Vx) and spanwise (Vy) velocity components. Figure 5(a) shows a 100 mm cut-line from a partial image of two chevrons, from which Vx and Vy profiles are extracted [Figs. 5(b) and 5(c)]. Vx fluctuates in sign, while Vy remains negative with lowest magnitude near the walls. Comparing with the sloped regions in Fig. 5(a), the existence of counterrotating vortices in the vicinity of chevrons can be inferred, as depicted schematically in Fig. 5(d).

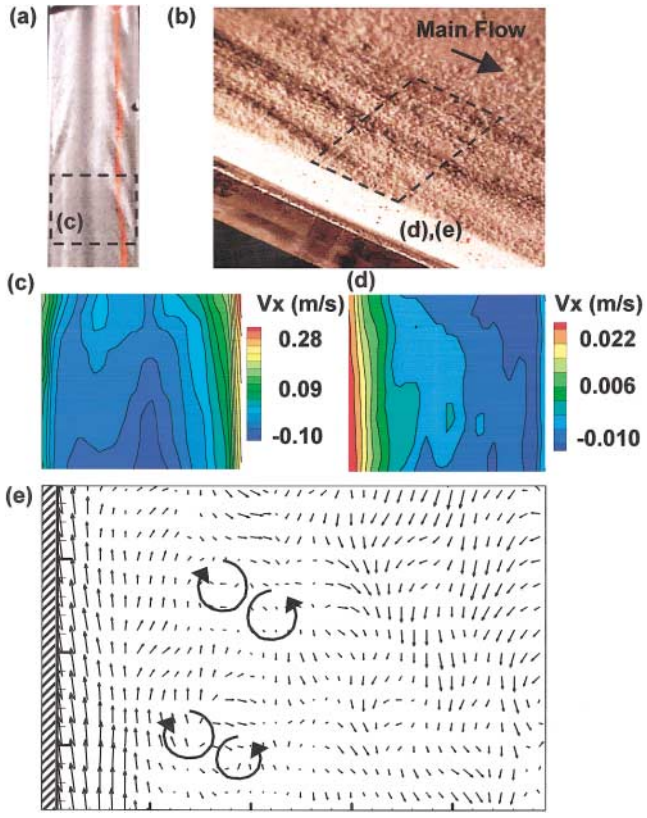

FIG. 4 (color). Chute flow images, $h = 6$ cm and mass flow $= 281 \pm 2$ g/s. Dashed lines indicate areas of PIV analyses. (a) width $= 7.6$ cm, $\theta = 27.1°$. Colored tracer particles (red) deflect towards walls. (b) Oblique view of side wall and neighboring free surface, width $= 20.4$ cm, $\theta = 24.3°$. (c) Mean streamwise velocity for narrow chute, averaged over 500 frames, each 76×60 mm; (d) streamwise velocity for wide chute, 500 frame average, 100×80 mm; (e) representative pseudoinstantaneous PIV vector plot for wide chute, averaged over 20 frames. In all PIV images, mean velocity is subtracted to emphasize fluctuations.

The experiments provide substantial evidence for subsurface circulation. The small surface outflows detected in the tracer experiments imply, by continuity, that there is a corresponding subsurface flow toward the centerline. We confirmed the importance of lateral flow by placing eight smooth wires, of diameter comparable to the particle size on one side of the centerline, flush with the bottom surface of the chute and parallel to the walls. In subsequent trials and for several θ, no chevrons (of either type) formed on that side of the chute, although they continued to be visible on the unaltered side. The wires were placed to prevent spanwise movement while minimally affecting streamwise flow, so these data tend to confirm the presence of subsurface circulation normal to the flow. The vorticity measured by PIV implies that each chevron consists of vortices tilted at an angle ϕ. Granular vortices previously observed in free-stream [6] and wall bounded flows [19] were not tilted, and were proposed to arise from granular temperature and density gradients. In the current case, buoyancy seems an unlikely driver because the chevrons materialize rapidly, without the previously reported induction lengths or times. Instead,

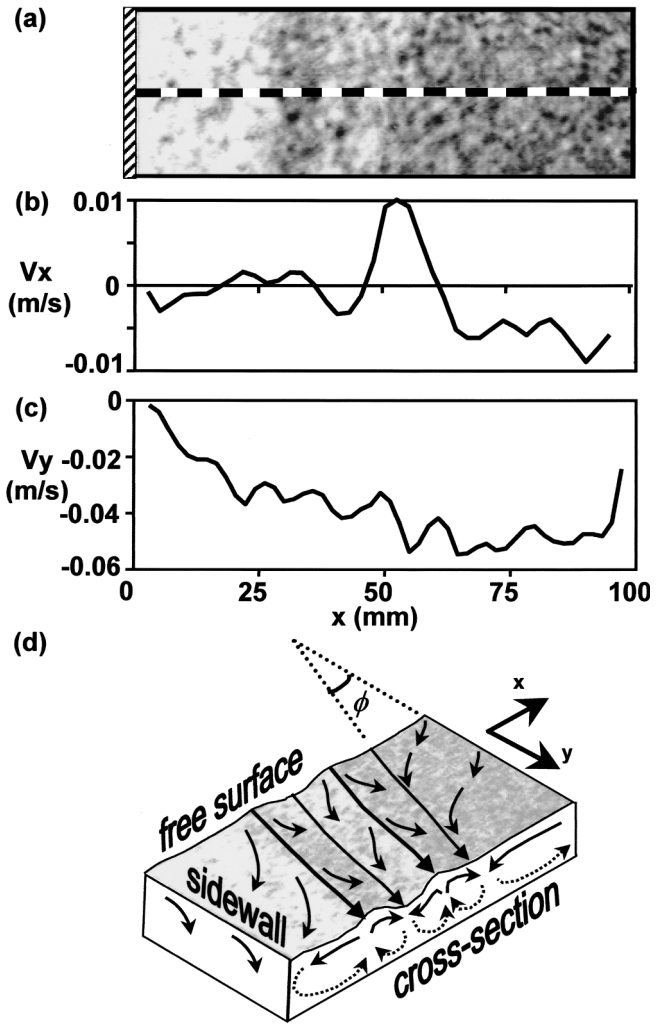

FIG. 5. (a) 35 × 100 mm image of free surface, bisecting two chevron waves. Left side of frame matches the left wall of the 20.4 cm-wide chute. Light areas slope to the left, dark areas to the right. PIV data for dotted cut-line is extracted to show (b) spanwise, and (c) streamwise velocity components, averaged over 50 frames. Mean vector = 0.146mm/s spanwise towards walls and −3.213 mm/s streamwise velocity. Standard deviation = 0.00103 and 0.00773 mm/s, respectively. (d) Schematic of granular bed section examined by PIV, showing measured velocity components (solid line) and inferred subsurface circulation (dotted line).

vortices appear to be induced directly by shear between frictional walls and the main flow, in the granular analog of a fluid boundary layer [20,21]. Steepening this velocity gradient (via increased wall roughness or chute slope) was shown to increase the vortex tilt angle ϕ. Our data are consistent with a tendency for the vortex direction to be always aligned perpendicular to the velocity gradient, with chevrons vanishing near the center of the chute where the gradient vanishes.

We have shown new wave patterns resulting from vortex development near boundaries for both accelerating and steady dense flows, where velocity gradients exist and sustained frictional contacts are expected. Vorticity was measured for one of the two observed wave types. Such circulation patterns may thus be present in a variety of industrially relevant flows near frictional boundaries, despite the absence of surface cues. It remains to be seen if underlying instabilities are intensified in the presence of highly frictional materials and more intense shear, perhaps sharing dynamical features with boundary layer fluids and renewing their significance for granular drag reduction and mixing applications.

We gratefully acknowledge the assistance of H. Salis, A. Hasan, J. Leung, E. Liss, K. Mehta, and J. Pantina. This work was supported by the NSF (CTS Division) and the ACS, Petroleum Research Fund. S. L. C. also wishes to thank Merck & Co., Inc. for financial support.

*Author to whom correspondence should be addressed.
†Present address: Schering-Plough Research Institute, Kenilworth, New Jersey 07033.

[1] S. B. Savage, J. Fluid Mech. **92**, 53 (1979).
[2] P. C. Johnson, P. Nott, and R. Jackson, J. Fluid Mech. **210**, 501 (1990).
[3] S. B. Savage, in *Theoretical and Applied Mechanics*, edited by P. Germain, M. Piau, and D. Caillerie (North-Holland, Amsterdam, 1989).
[4] O. Pouliquen, J. Delour, and S. B. Savage, Nature (London) **386**, 816 (1997).
[5] M. Y. Louge and S. C. Keast, Phys. Fluids **13**, 1213 (2001).
[6] Y. Forterre and O. Pouliquen, Phys. Rev. Lett. **86**, 5886 (2001).
[7] D. J. Goldfarb, B. J. Glasser, and T. Shinbrot, Nature (London) **415**, 302 (2002).
[8] A. Daerr, Phys. Fluids **13**, 2115 (2001).
[9] O. Pouliquen and Y. Forterre, J. Fluid Mech. **453**, 133 (2002).
[10] J. Rajchenbach, Phys. Rev. Lett. **88**, 014301 (2002).
[11] T. Herbert, Annu. Rev. Fluid Mech. **20**, 487 (1988).
[12] C. D. Donaldson and R. S. Snedeker, J. Fluid Mech. **45**, 281 (1971).
[13] C. Davies, G. Weir, and P. McGavin, Powder Technol. **106**, 1 (1999).
[14] S. N. Prasad, D. Pal, and M. J. M. Romkens, J. Fluid Mech. **413**, 89 (2000).
[15] A. Q. Shen, Phys. Fluids **14**, 462 (2002).
[16] C. H. K. Williamson, J. Fluid Mech. **206**, 579 (1989).
[17] P. J. Lamont and B. L. Hunt, J. Fluid Mech. **100**, 471 (1980).
[18] D. Chirichella *et al.*, Phys. Fluids **14**, 781 (2002).
[19] S.-S. Hsiau, P. C. Wang, and C.-H. Tai, AIChE J. **48**, 1430 (2002).
[20] R. M. Nedderman and C. Laohukal, Powder Technol. **25**, 91 (1980).
[21] D. Mueth *et al.*, Nature (London) **406**, 385 (2000).